



Preclinical PET imaging with the novel human antibody ⁸⁹Zr-DFO-REGN3504 sensitively detects PD-L1 expression in tumors and normal tissues

Marcus P Kelly , Sosina Makonnen, Carlos Hickey, T Cody Arnold, Jason T Giurleo, Richard Tavaré, Makenzie Danton, Christian Granados, Ishita Chatterjee, Drew Dudgeon , Marc W Retter, Dangshe Ma, William C Olson, Gavin Thurston, Jessica R Kirshner

To cite: Kelly MP, Makonnen S, Hickey C, *et al*. Preclinical PET imaging with the novel human antibody ⁸⁹Zr-DFO-REGN3504 sensitively detects PD-L1 expression in tumors and normal tissues. *Journal for ImmunoTherapy of Cancer* 2021;9:e002025. doi:10.1136/jitc-2020-002025

► Additional material is published online only. To view please visit the journal online (<http://dx.doi.org/10.1136/jitc-2020-002025>)

Accepted 15 December 2020



© Author(s) (or their employer(s)) 2021. Re-use permitted under CC BY-NC. No commercial re-use. See rights and permissions. Published by BMJ.

Regeneron Pharmaceuticals Inc, Tarrytown, New York, USA

Correspondence to

Dr Marcus P Kelly;
marcus.kelly@regeneron.com

ABSTRACT

Background Programmed cell death protein 1/programmed death-ligand 1 (PD-1/PD-L1) blocking antibodies including cemiplimab have generated profound clinical activity across diverse cancer types. Tumorous PD-L1 expression, as assessed by immunohistochemistry (IHC), is an accepted predictive marker of response to therapy in some cancers. However, expression is often dynamic and heterogeneous, and therefore not reliably captured by IHC from tumor biopsies or archival samples. Thus, there is significant need for accurate whole-body quantification of PD-L1 levels.

Methods We radiolabeled the novel human anti-PD-L1 antibody REGN3504 with zirconium-89 (⁸⁹Zr) using the chelator p-SCN-Bn-Deferoxamine to enable non-invasive immuno-positron emission tomography (immuno-PET) of PD-L1 expression. PET imaging assessed the localization of ⁸⁹Zr-REGN3504 to multiple human tumor xenografts. Mice genetically humanized for PD-1 and PD-L1 were used to assess the biodistribution of ⁸⁹Zr-REGN3504 to normal tissues and the estimated human radiation dosimetry of ⁸⁹Zr-REGN3504 was also determined. Pharmacokinetics of REGN3504 was assessed in monkeys.

Results Clear localization of ⁸⁹Zr-REGN3504 to human tumor xenografts was observed via PET imaging and ex vivo biodistribution studies demonstrated high (fourfold to sixfold) tumor:blood ratios. ⁸⁹Zr-REGN3504 specifically localized to spleen and lymph nodes in the PD-1/PD-L1 humanized mice. ⁸⁹Zr-REGN3504 immuno-PET accurately detected a significant reduction in splenic PD-L1 positive cells following systemic treatment with clodronate liposomes. Radiation dosimetry suggested absorbed doses would be within guidelines for other ⁸⁹Zr radiolabeled, clinically used antibodies. Pharmacokinetics of REGN3504 was linear.

Conclusion This work supports the clinical translation of ⁸⁹Zr-REGN3504 immuno-PET for the assessment of PD-L1 expression. Future clinical studies will aim to investigate the utility of ⁸⁹Zr-REGN3504 immuno-PET for predicting and monitoring response to anti-PD-1 therapy.

BACKGROUND

Checkpoint inhibitor (CPI) immunotherapy has led to a paradigm shift in the clinical

management of many cancers and exemplified the promise of cancer immunotherapy to lead to deep and durable anti-tumor activity in patients refractive to various prior therapies.^{1,2} Antibodies blocking the programmed cell death protein 1 (PD-1) and programmed death-ligand 1 (PD-L1) inhibitory signaling axis are the most prominent class of CPI therapy and have advanced into front-line treatments in cancers such as non-small cell lung cancer (NSCLC).^{3,4}

As interaction of PD-1 on T Cells with PD-L1 expressed on tumor cells and other cell populations mediates the inhibitory signaling of T Cells, expression of PD-L1 has been investigated as a putative biomarker of cancers most likely to respond to antibodies interrupting this signaling.⁵⁻⁷ In early clinical development of anti-PD-1 antibody nivolumab, patients with tumors including NSCLC, melanoma and renal-cell cancer that exhibited greater than 5% PD-L1 positivity by immunohistochemistry (IHC) had a 36% objective response rate, whereas no objective responses were seen in patients who were PD-L1 negative.⁸ Further mechanistic studies by Taube *et al* demonstrated that PD-L1 expression was the most predictive biomarker of anti-PD-1 therapy response relative to other markers including PD-1 and PD-L2.⁹ The KEYNOTE-001 and KEYNOTE-010 clinical trials assessing anti-PD-1 pembrolizumab in advanced NSCLC further validated the apparent association between response to PD-1 blockade and PD-L1 expression, as patients whose tumors had ≥50% PD-L1 positivity by IHC were observed to have greater clinical benefit relative to patients with lower PD-L1 expression.^{5,10} The correlation of greater PD-L1 expression to clinical response

in additional trials resulted in the approval of pembrolizumab for the treatment of first-line NSCLC in patients whose tumors expressed $\geq 50\%$ PD-L1 by IHC.¹¹

Despite the apparent importance of PD-L1 expression in predicting response, further clinical development of PD-1/PD-L1 therapeutics has illustrated various cases where patients with seemingly PD-L1 negative tumors demonstrated significant responses to these therapeutics.^{11–14} Conversely, patients whose tumors have demonstrated high PD-L1 expression have demonstrated a lack of clinical benefit following PD-1/PD-L1 immunotherapy.^{2 5 15} Such results may highlight some inherent limitations of biopsy-based IHC assays in the accurate assessment of PD-L1 expression in patients.¹⁶ The most apparent of these is that biopsy-based techniques generally only sample from a small, single site that does not accurately capture the marked inter-lesion and intra-lesion heterogeneity of PD-L1 expression across multiple tumor sites that has been observed in more detailed studies of PD-L1 expression.^{9 17–20} Further, despite efforts to harmonize assessment of PD-L1 expression across various staining and analysis platforms, possible misclassification of PD-L1 expression has been found to occur in up to 37% of patients, a finding that could result in the unintentional withholding of treatment.^{16 21} Lastly, changes over time in PD-L1 expression are known to be induced by factors such as radiotherapy and other treatments, and through alterations to the tumor microenvironment.^{22–24} Subsequently, the assessment of PD-L1 on archival tissue samples may not align with the contemporaneous expression of PD-L1 during CPI immunotherapy. These issues with IHC-based assays of PD-L1 provide an opportunity to explore alternate methodologies, with the possibility that improvements to the assessment of PD-L1 expression may also provide insight into whether other immune signaling pathways limit the response to anti-PD-1/PD-L1 therapy.

Molecular imaging techniques including immuno-positron emission tomography (immuno-PET) may address some of the limitations of histology-based techniques and serve as a complementary modality in the assessment of PD-L1 expression and other cancer biomarkers.^{16 25–27} Immuno-PET is a whole-body imaging technique that combines the sensitivity and quantitation of PET imaging with the high-affinity specific targeting of antibodies and other antibody-based molecules.^{28–31} One clear advantage of using immuno-PET is that it allows for the non-invasive visualization of all antibody accessible antigen-positive tissues, allowing for the assessment of antigen expression on normal tissues and determining the extent of heterogeneous expression across tumors and normal tissues.^{32–34} Anatomical registration to tissues is performed using concurrently acquired CT or MRI imaging. Immuno-PET allows for the quantitative assessment of current PD-L1 expression in patients undergoing therapy and it can potentially be performed longitudinally to capture changes in expression over time.^{16 26} Importantly, successful translation of preclinical

immuno-PET studies have been observed for multiple antibodies targeting both traditional tumor markers and immunotherapy targets.^{16 25 31}

As accurate detection of PD-L1 expression could serve as a predictive biomarker to select patients for anti-PD-1/PD-L1 therapies, we characterized a zirconium-89 (⁸⁹Zr) radiolabeled fully human anti-human PD-L1 antibody, ⁸⁹Zr-DFO-REGN3504, for use as an immuno-PET agent. Our results demonstrate that ⁸⁹Zr-DFO-REGN3504 immuno-PET sensitively detects the expression of human PD-L1 in tumors and in the normal tissues of mice engineered to express human PD-L1. Overall, our results support the clinical investigation of ⁸⁹Zr-DFO-REGN3504 to assess the expression of PD-L1 in patients undergoing CPI immunotherapy.

METHODS

Cell lines

NCI-H441 (HTB-174), MDA-MB-231 (HTB-26) and HCC827 (CRL-2868) human tumor cells were purchased from the American Type Culture Collection (ATCC). Cell lines were authenticated at the ATCC by short-tandem repeat profiling. NCI-H441 and HCC827 cells were cultured in RPMI 1640 medium supplemented with 10% v/v fetal calf serum. MDA-MB-231 were cultured in Leibovitz's L-15 Medium supplemented with 10% v/v fetal calf serum. MC-38 cells were obtained from the NCI (National Cancer Institute) - Laboratory of Tumor Immunology and Biology (designator 'Colon 38'). The expression of murine PD-L1 was disrupted in these cells using CRISPR/Cas9 technology and the cells were subsequently engineered to stably express human PD-L1. MC-38 were cultured in DMEM supplemented with 10% v/v fetal bovine serum.

Generation of REGN3504 and DFO-REGN3504

REGN3054 was produced using the VelocImmune mice platform, where mouse immunoglobulin heavy and kappa light variable regions are replaced with their human counterparts while leaving the mouse constant regions intact.³⁵ VelocImmune mice were immunized with the extracellular domain of human PD-L1. Spleens were harvested for generation of hybridomas or for direct isolation of antigen-binding splenocytes. The REGN3504 immunoglobulin contains a human light chain variable domain fused to a human kappa constant domain and a human heavy chain variable region fused to a human IgG4 constant domain. The IgG4 constant domain contains a serine to proline amino acid substitution (S228P) in the hinge region to promote stabilization of disulfide bonds between the two heavy chains and minimize half-antibody formation. Antibodies were produced in Chinese hamster ovary cells. To generate DFO-REGN3504, purified antibody was incubated under basic conditions with a threefold molar excess of *p*-SCN-Bn-DFO bifunctional chelator for 30 min at 37°C, yielding DFO-REGN3504 with an average DFO to antibody ratio of

1.5. Control IgG4 DFO immunoconjugate was produced under similar conditions.

Molecular characterization of REGN3504 and DFO-REGN3504

An ELISA-based binding assay was developed to assess the binding of REGN3504 and DFO-REGN3504 to immobilized human or cynomolgus monkey PD-L1. Recombinant human or monkey PD-L1.mFc was diluted to 1 µg/mL in phosphate-buffered saline (PBS) and passively absorbed to microtiter plates overnight at 4°C. REGN3504 or Control antibody together with the respective DFO immunoconjugates were then added in duplicate to the PD-L1 coated plates at concentrations ranging from 51 fM to 3 nM. Following a 1 hour incubation at room temperature, bound antibody or DFO immunoconjugate was detected with (HRP)-conjugated goat anti-human Fcγ antibody (in 1:5000 dilution) and visualized using the colorimetric HRP-substrate, 3,3',5,5'-tetramethylbenzidine (TMB) according to the manufacturer's protocol. Absorbance at 450 nm was recorded and plotted as a function of antibody or immunoconjugate concentration. Binding data were analyzed using a 4-parameter logistic equation over an 11-point response curve with GraphPad Prism software and EC₅₀ values were calculated.

An ELISA-based blocking assay was employed to determine the ability of REGN3504 and DFO-REGN3504 to block the interaction of a constant concentration of human or monkey PD-L1 to immobilized recombinant human PD-1 or CD80. To determine EC₅₀ values for PD-L1 binding to PD-1 or CD80, human PD-1 or CD80 was diluted to 2 µg/mL in PBS and passively absorbed to microtiter plates overnight at 4°C. Recombinant human or monkey PD-L1.mFc was then added in duplicate at 1.69 pM - 0.1 µM for PD-1 or 16.9 pM - 1.0 µM for CD80. Following a 1 hour incubation at room temperature, bound PD-L1.mFc was detected with HRP-conjugated goat anti-mouse Fcγ antibody (1:5000 dilution) and visualized using TMB according to the manufacturer's recommended protocol. Absorbance at 450 nm was recorded and plotted as a function of PD-L1.mFc concentration. Binding data were analyzed using a 4-parameter logistic equation over an 11-point response curve with GraphPad Prism software and EC₅₀ values were calculated. To determine IC₅₀ values for REGN3504 or DFO-REGN3504 blocking of PD-L1 to PD-1 or CD80, the recombinant human or monkey PD-L1.mFc at 500 pM for PD-1 or 10 nM for CD80 were mixed with REGN3504, Control antibody or the respective DFO immunoconjugates. For PD-1, 9.76 pM - 10 nM antibody/DFO-immunoconjugate was assessed and 4.23 pM - 0.25 µM antibody/DFO-immunoconjugate was used for human PD-L1.mFc interaction with CD80. Antibody/DFO-immunoconjugate at 16.9 pM - 1.0 µM was used to assess monkey PD-L1.mFc interaction with CD80. The antibody and PD-L1.mFc mixtures were then transferred to PD-1 or CD80 coated microtiter plates in duplicate. Following a 1 hour incubation at room temperature, bound PD-L1.mFc was detected as described above. The binding data were plotted as a function of antibody or

DFO-immunoconjugate concentrations and analyzed using a 4-parameter logistic equation over an 11-point response curve with GraphPad Prism software and IC₅₀ values of blocking PD-L1 binding to PD-1 or CD80 were calculated.

The affinities of REGN3504 and DFO-REGN3504 for human and monkey PD-L1 were measured in surface plasmon resonance (SPR) experiments performed on a Biacore T200 instrument using a dextran-coated (CM5) chip at 37°C. Antibodies were captured by mouse anti-human Fcγ antibody immobilized on the sensor chips and were tested for binding to the extracellular domains of human and monkey PD-L1 in monomeric format. PD-L1 proteins ranging from 0.31 to 10.0 nM were injected over the captured REGN3504 or DFO-REGN3504 surfaces. The kinetic parameters were obtained by globally fitting these specific sensorgrams to a 1:1 binding model with mass transport limitation using Biacore T200 evaluation software V.2.0. The equilibrium dissociation constant (K_D) was calculated from the ratio of the dissociation rate constant to the association rate constant ($K_D = k_d/k_a$).

Radiolabeling of REGN3504

Anti-PD-L1 radioimmunoconjugate (⁸⁹Zr-DFO-REGN3504) or isotope control radioimmunoconjugate were prepared by complexation of (⁸⁹Zr)Zr-oxalate with anti-PD-L1 immunoconjugate (DFO-REGN3504) or isotope control immunoconjugate. (⁸⁹Zr)Zr-oxalate (37–111 MBq) in 1 M oxalic acid was adjusted to a volume of 1 mL with 1 M HEPES buffer, pH 7.4. Next, 200 µL of immunoconjugate in 1M HEPES, pH 7.4 was added, mixed, and incubated at room temperature (RT) for 45 min to allow for complexation. Reaction mixtures were then added to PD-10 columns that had been equilibrated with 25 mL of 250 mM sodium acetate (NaOAc), pH 5.4 for gravity-fed desalting. Radioimmunoconjugates were eluted in 1.8 mL NaOAc, pH 5.4 and stored at RT. For simplicity, ⁸⁹Zr-DFO-REGN3504 will be abbreviated to ⁸⁹Zr-REGN3504 throughout this study.

Tumor xenografts and dosing

Tumor xenografts for subsequent immuno-PET studies were established in male C.B.-17 SCID mice (Taconic Biosciences). For the NCI-H441, MDA-MB-231 and HCC827 xenografts, mice were implanted with 5×10⁶ cells into the flank. Tumors were measured with calipers two times a week until tumor volume reached approximately 150 mm³. MC-38/hPD-L1 tumors were established following injection of 1×10⁶ cells into the flank of PD-1/PD-L1 humanized mice. MC-38/hPD-L1 tumors were measured with calipers two times a week until tumor volume reached approximately 50 mm³. At this time, animals were randomized into n=4 to 5 treatment groups and ⁸⁹Zr-REGN3504 or ⁸⁹Zr-IgG4 control were administered by intravenous tail-vein injection at the doses outlined in the results. In all studies, further unlabeled REGN3504 was added to the initial constant dose of ⁸⁹Zr-REGN3504 in order to achieve higher overall antibody

doses. For the depletion of macrophages via the administration of clodronate liposomes, mice were administered Clophosome-A or Control liposomes (FormuMax) at 8 µl/g. All procedures were conducted according to the guidelines of the Regeneron Institutional Animal Care and Use Committee.

Generation of double-humanized PD-1/PD-L1 mice

Mice expressing both human PD-1 and human PD-L1 were generated by breeding the two respective strains of single-humanized PD-1 and PD-L1 animals. These humanized mice strains were generated using VelociGene technology at Regeneron Pharmaceuticals.^{36,37} Generation of PD-1 humanized mice were previously described by Burova *et al.*³⁸. Single-humanized PD-L1 mice were generated in which a portion of the mouse PD-L1 gene encoding the extracellular domain was replaced with a fragment of human-PD-L1 gene encoding the extracellular domain of human PD-L1. This resulted in the generation of a chimeric transmembrane protein comprising the human extracellular domain that can be bound by REGN3504 and the ⁸⁹Zr-REGN3504 radioimmunoconjugate.

In vivo immuno-PET imaging

PET imaging to assess in vivo radioimmunoconjugate localization was performed 6 days after administration of ⁸⁹Zr-REGN3504 or ⁸⁹Zr-IgG4 control. A Sofie Biosciences G8 PET/CT instrument (Sofie Biosciences and PerkinElmer) was used to acquire images. The instrument was calibrated for detection of ⁸⁹Zr prior to image acquisition. The energy window ranged from 150 to 650 keV with a reconstructed resolution of 1.4 mm at the center of the field of view. Mice underwent induction anesthesia using isoflurane and were kept under continuous flow of isoflurane during imaging. Static images were acquired for 10 min using the G8 acquisition software and subsequently reconstructed using pre-configured settings. Image data was corrected for decay and other parameters. CT images were acquired following PET acquisition and later co-registered with the corresponding PET images. Images were processed using VivoQuant post-processing software (Invivo Imaging Services). PET imaging raw data were converted into false-colored maximum intensity projections on a color scale calibrated to indicate a signal range of 0% to 30% of injected dose per volume, expressed as %ID/g.

Ex vivo biodistribution

For ex vivo biodistribution analysis, mice were euthanized following the imaging procedure on day 6 post dosing. Blood was collected via cardiac puncture into counting tubes. Tumors and select normal tissues (spleen, heart, lungs, stomach, intestine (small), liver, kidneys, and bone (femur)) were then excised and placed into counting tubes. The weight of each sample (blood, tumor, or tissues) was measured and recorded. Values for ⁸⁹Zr 511 keV photons were then determined in counts per minute (cpm) by measuring samples using an automatic gamma

counter (Wizard 2470, PerkinElmer). Samples from some studies were weighed and counted using an Hidex Automatic Gamma Counter (Hidex, Finland). The %ID values for individual samples collected were calculated relative to the 511 keV photons count value for a dose-standard from injected material prepared on the day of dosing and measured on day 6 post dosing:

$$\%ID = \frac{511 \text{ keV photons of sample on day 6 post dosing (cpm)}}{511 \text{ keV photons of dose standard on day 6 post dosing (cpm)}} \times 100$$

Subsequently, the %ID/g values were derived using the weight of the individual samples and the ratio of tissue (or tumor)-to-blood %ID/g values was calculated for each sample.

Dosimetry estimates

In order to estimate the radiation exposures in human subjects following administration of ⁸⁹Zr-REGN3504, dosimetry values were derived from tumor-free PD-1/PD-L1 humanized mice that received 1 mg/kg (1.85 MBq) ⁸⁹Zr-REGN3504. Longitudinal immuno-PET imaging data at 1, 24, 48, 72 and 144 hours post dosing were used for the dosimetry calculations. Tissue concentration values of ⁸⁹Zr-REGN3504 was determined by volume of interest (VOI) analysis. Detailed methods of the dosimetry calculations are outlined in the online supplemental material 1.

Pharmacokinetic analysis of REGN3504

Fifteen female cynomolgus monkeys (five animals/group) received a single intravenous infusion of 1, 5, or 15 mg/kg REGN3504. Blood samples for the determination of functional REGN3504 concentrations in serum were collected from all animals prior to dosing and at 0.083 (5 minutes post the 30 min infusion), and from 12 hours through 1344 hours (8 weeks) post dose. Concentrations of functional REGN3504 in cynomolgus monkey serum were measured using a validated ELISA; this method employed microtiter plates coated with a recombinant protein containing the extracellular domain of human PD-L1 as the capture reagent. REGN3504 captured on the plate is detected using a biotinylated mouse anti-human IgG4 monoclonal antibody, followed by NeutrAvidin conjugated with horseradish peroxidase. A luminol-based substrate specific for peroxidase is then added to generate a signal whose intensity is proportional to the concentration of functional REGN3504. The lower limit of quantitation is 0.078 µg/mL in neat monkey serum.

Concentrations of functional REGN3504 were analyzed by non-compartmental analysis (NCA) using Phoenix, WinNonlin (V,6.4, Certara, LP) using a constant infusion model. Linear trapezoidal rule and linear interpolation with uniform weighting were used in model settings. The target dose(s) of REGN3504, as described in the study protocol, were used in NCA; the actual administered doses were within 10% of the target dose.

Statistical analysis

Statistical analyzes were performed utilizing GraphPad Prism 7.0 software. Comparison of antibody dose groups were assessed using unpaired non-parametric Welch's t-testing. A threshold of $p < 0.05$ was considered statistically significant.

RESULTS

High affinity binding of REGN3504 to PD-L1 and inhibition of PD-1 and CD80 binding to PD-L1 by REGN3504 is not affected by conjugation to DFO

The binding of antibody REGN3504 and DFO conjugated DFO-REGN3504 to both human and cynomolgus monkey PD-L1 was determined by direct-binding ELISA. As shown in [figure 1A and B](#), both REGN3504 and DFO-REGN3504 demonstrated concentration-dependent binding to PD-L1-Fc. For human PD-L1, REGN3504 and DFO-REGN3504 bound with EC_{50} values of 41.1 and 46.8 pM, respectively ([figure 1A](#)). No PD-L1 binding was observed using either control antibody or DFO-IgG4 control immunconjugate. REGN3504 and DFO-REGN3504 bound to cynomolgus monkey PD-L1 with EC_{50} values of 47.7 and 51.0 pM, respectively ([figure 1B](#)). Overall, binding of either REGN3504 or DFO-REGN3504 was similar between species with the EC_{50} values within 1.1-fold to 1.2-fold of each other. Conjugation of REGN3504 with DFO resulted in little or no change to binding.

The binding affinity of both REGN3504 and DFO-REGN3504 were also assessed by SPR technology. Unconjugated REGN3504 demonstrated high affinity binding for monomeric human and monkey PD-L1 with equilibrium dissociation constants (K_D) values of 260 pM and 284 pM, respectively. DFO-REGN3504 immunconjugate similarly demonstrated high affinity binding for monomeric human and monkey PD-L1 with equilibrium dissociation constants (K_D) values of 389 pM and 481 pM, respectively. The DFO-REGN3504 K_D values were within 1.7-fold of REGN3504 values, indicating that conjugation of antibody with the DFO chelate did not significantly affect the binding to PD-L1. Neither REGN3504 nor DFO-REGN3504 demonstrated any binding to mouse or rat PD-L1.

The ability of REGN3504 and DFO-REGN3504 to block the interaction of PD-L1 and PD-1 were determined by ELISA ([figure 1C and D](#)). This assay measured the capacity of varying antibody concentrations to block the interaction between a fixed concentration of PD-L1 to immobilized PD-1. Human and monkey PD-L1 bound immobilized human PD-1 with EC_{50} values of 741 pM and 2.88 nM, respectively. REGN3504 and DFO-REGN3504 demonstrated a similar ability to block binding of 500 pM of human PD-L1 to immobilized PD-1, with IC_{50} values of 243 pM and 266 pM, respectively ([figure 1C](#)). REGN3504 and DFO-REGN3504 blocked binding of 500 pM of monkey PD-L1 to immobilized PD-1, with IC_{50} values of 162 pM and 178 pM, respectively ([figure 1D](#)). The ability of REGN3504 and DFO-REGN3504 to block

the interaction of 10 nM PD-L1 to immobilized CD80 was also assessed. REGN3504 and DFO-REGN3504 blocked the interaction of human PD-L1 and CD80 with IC_{50} values of 4.38 nM and 5.12 nM, respectively ([figure 1E](#)). REGN3504 and DFO-REGN3504 blocked the interaction of monkey PD-L1 and human CD80 with IC_{50} values of 4.22 nM and 5.63 nM, respectively ([figure 1F](#)).

^{89}Zr -REGN3504 demonstrates high immunoreactivity and purity

Following each chelation of ^{89}Zr to DFO-REGN3504, the resulting radioimmunoconjugate was characterized to ensure that it retained specific binding to PD-L1. The immunoreactivity of ^{89}Zr -REGN3504 was assessed by single point binding assay. Average immunoreactivity of $93.4 \pm 5\%$ was observed from the radiolabeling employed in this study. SEC-HPLC was used to determine the monomeric purity and radiochemical purity of ^{89}Zr -REGN3504, with these averaging $>99\%$ and $96.6 \pm 1.6\%$ (online supplemental figure 1 and online supplemental table 1).

^{89}Zr -REGN3504 specifically detects the expression of PD-L1 on human tumor xenografts in vivo

To validate the ability of ^{89}Zr -REGN3504 to detect PD-L1 expression, human cancer cells with varying levels of PD-L1 expression were developed as xenografts. Expression of PD-L1 was generally moderate in the cell lines as assessed by flow cytometry and low when assessed by PD-L1 immunohistochemistry of tumor xenografts (online supplemental figures 2 and 3). Representative PET/CT images of mice injected with 0.1 mg/kg ^{89}Zr -REGN3504 or ^{89}Zr -IgG4 control Ab, and the associated ex vivo biodistribution data, are shown in [figure 2](#). Images at early times following intravenous dosing revealed distribution of the antibodies to the heart and major vessels. Over time, marked ^{89}Zr -REGN3504 localization to tumors was observed in all of the models. As assessed by %ID/g, uptake was highest in NCI-H441 tumors at 52.3 %ID/g, which was 4.6-fold over the ^{89}Zr -REGN3504 blood level. Uptake in HCC827 tumors was 38.7 %ID/g which was 5.9-fold above blood levels. Lastly, uptake in MDA-MB-231 tumors was 38.8 %ID/g, 3.9-fold over blood levels. Uptake of ^{89}Zr -REGN3504 was significantly higher than ^{89}Zr -IgG4 control antibody across all three tumor models (NCI-H441; $p = 0.0002$, HCC827; $p = 0.0008$, MDA-MB-231; $p < 0.0001$). Administration of ^{89}Zr -REGN3504 with additional unlabeled REGN3504 (totaling 0.5 or 5.0 mg/kg REGN3504) led to a dose dependent reduction in tumor localization due to competition for PD-L1 binding between ^{89}Zr -REGN3504 and unlabeled REGN3504 ([figure 2](#), online supplemental figure 4).

The sensitivity of ^{89}Zr -REGN3504 for detection of PD-L1 positive tumors was further demonstrated in a model of lung metastasis established using intravenous injection of MDA-MB-231 cells. Here, ^{89}Zr -REGN3504 was able to specifically localize to small tumors in the lungs of mice,

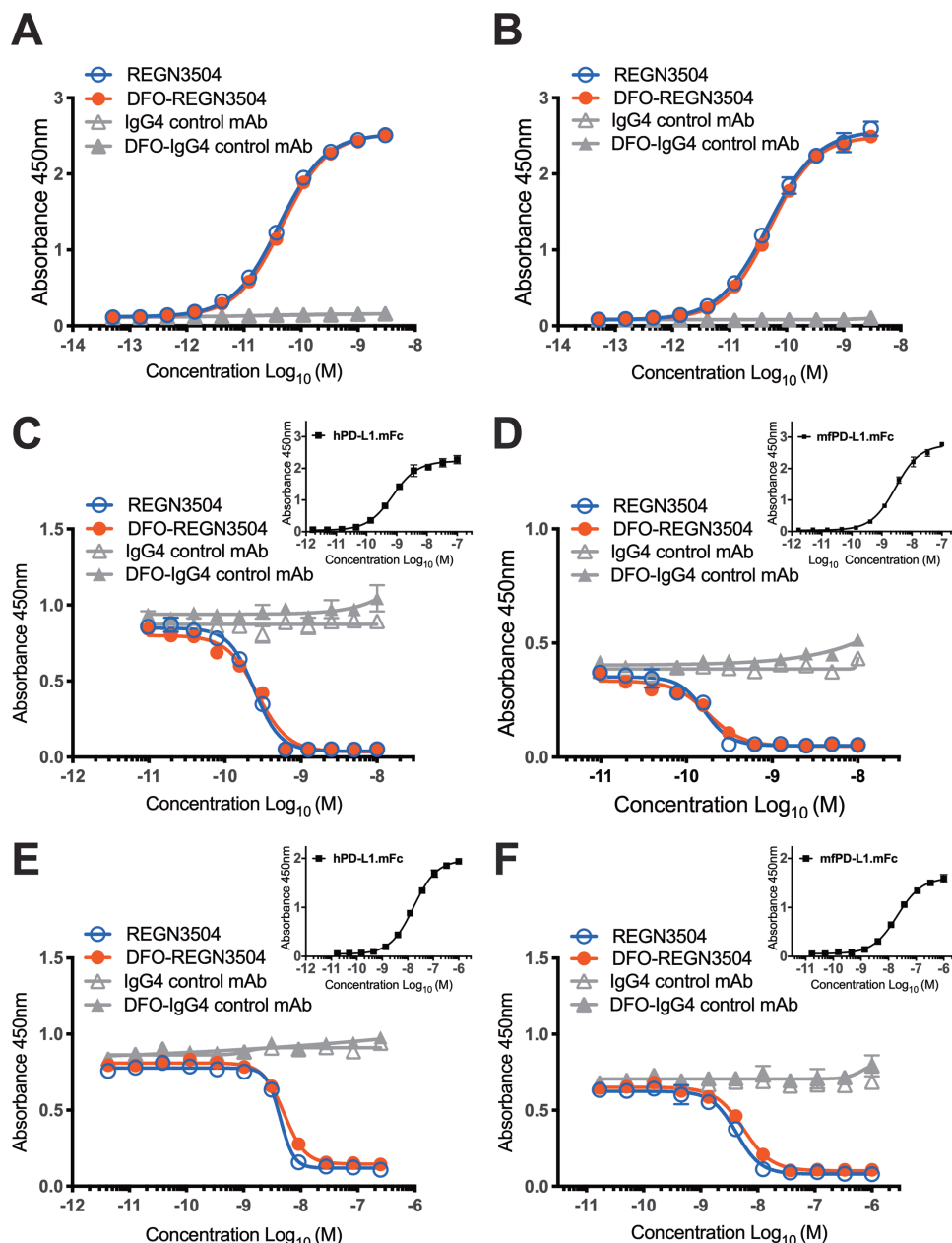


Figure 1 REGN3504 and DFO-REGN3504 bind human and cynomolgus monkey PD-L1 and block the binding of human and cynomolgus monkey PD-L1 to PD-1 and CD80. Binding of REGN3504 and DFO-REGN3504 to immobilized human (A: hPD-L1.mFc) or cynomolgus monkey (B: MfPD-L1.mFc) PD-L1 was evaluated by ELISA. REGN3504 (blue, open circles) and DFO-REGN3504 (red, filled circles) at a range of concentrations (51 fM to 3 nM). Under identical assay conditions, isotype control antibody (gray, open triangles) and isotype DFO-IgG4 control immunoconjugate (gray, filled triangles) did not bind PD-L1. Representative data from an assay performed in duplicate wells are presented as mean \pm SD. ELISA-based methods were used to assess REGN3504 and DFO-REGN3504 concentration-dependent blocking of the binding of a constant concentration of human (C, E: hPD-L1.mFc) or cynomolgus monkey (D, F: MfPD-L1.mFc) PD-L1 to immobilized human PD-1 (C, D: hPD-1) or CD80 (E, F: CD80). In each format, four articles were tested: REGN3504 (blue, open circles), DFO-REGN3504 (red, filled circles), isotype control antibody (gray, open triangles), or isotype DFO-IgG4 control immunoconjugate (gray, filled triangles). Binding curves for PD-L1.mFc (black filled squares) binding to immobilized hPD-1 or hCD80 are shown as insets in C-F. No blocking was observed with isotype control antibody and immunoconjugate under the identical respective assay conditions. Representative data from an assay performed in duplicate wells are presented as mean \pm SD. PD-1, programmed cell death protein 1; PD-L1, programmed death-ligand 1.

as observed in PET/CT images (online supplemental figure 5). Overall, these results demonstrate specific and sensitive detection of ⁸⁹Zr-REGN3504 in PD-L1 positive tumors by immuno-PET.

⁸⁹Zr-REGN3504 demonstrates localization to normal lymphoid tissues in mice humanized for PD-L1 and PD-1

As REGN3504 does not bind to murine PD-1, we used VelociGene mice genetically humanized for both PD-L1

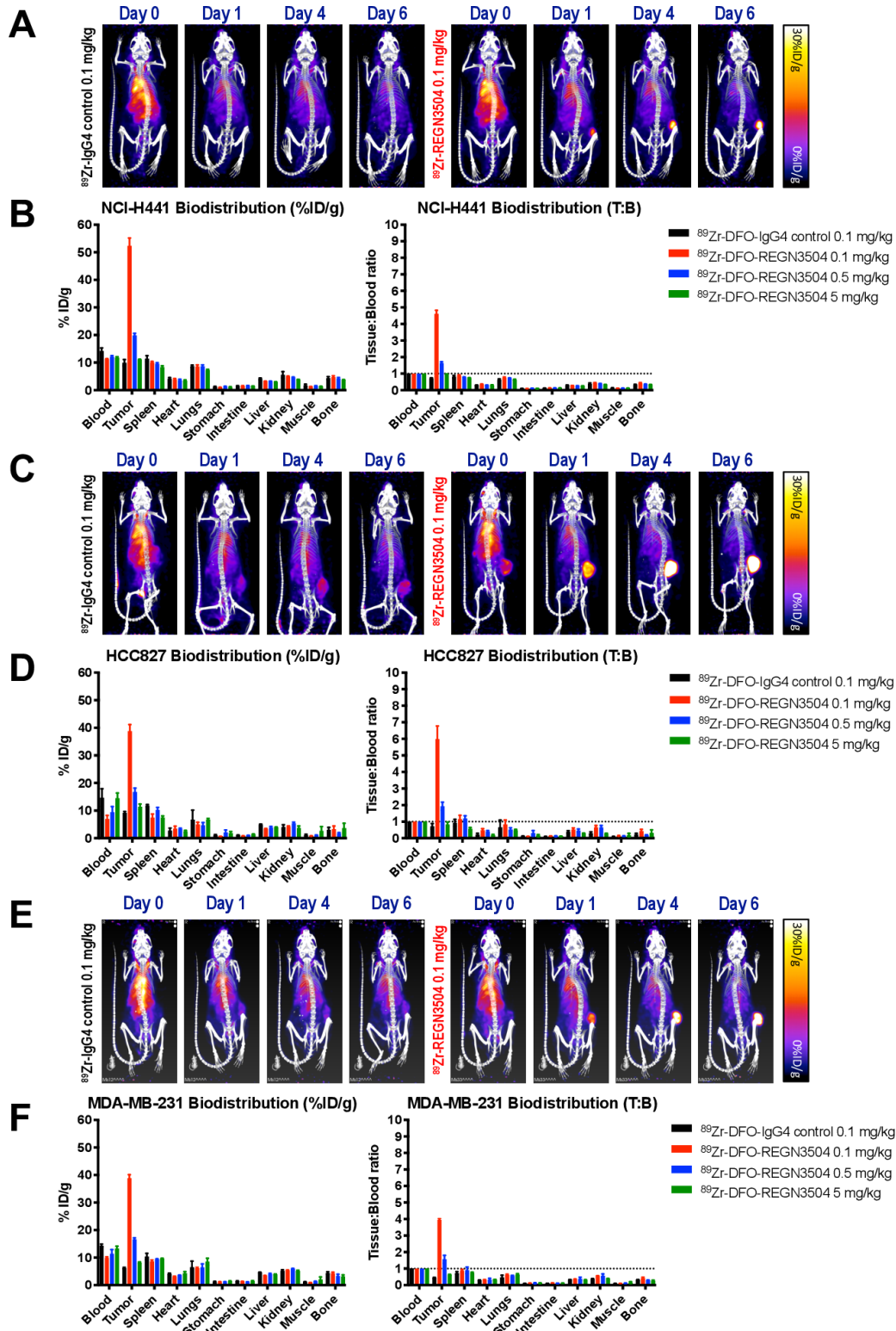


Figure 2 ^{89}Zr -REGN3504 demonstrates specific localization to human PD-L1 positive tumor xenografts. The tumor localization and biodistribution of ^{89}Zr -REGN3504 was assessed in SCID mice bearing human tumor xenografts ($n=4/\text{group}$). Animals received a single intravenous injection of ^{89}Zr -IgG4 control or ^{89}Zr -REGN3504 and PET/CT images were acquired on Day 0, 1, 4 and 6 Days post injection. On Day 6 post injection, quantitative ex vivo biodistribution was performed. Representative PET/CT images demonstrate the localization of ^{89}Zr -IgG4 control or ^{89}Zr -REGN3504 over time in mice bearing NCI-H441 (A), HCC827 (B) and MDA-MB-231 (C), respectively. The biodistribution of ^{89}Zr -IgG4 control (0.1 mg/kg) or ^{89}Zr -REGN3504 (0.1, 0.5 and 5 mg/kg) presented as per cent injected dose per gram (%ID/g) or tissue-to-blood ratio (T:B) is shown for NCI-H441 (B), HCC827 (D) and MDA-MB-231 (F) tumor-bearing animals, respectively. The administered radioactivity dose was 1.7, 1.33 and 1.48 MBq for ^{89}Zr -IgG4 control and 1.66, 1.33 and 1.48 MBq for ^{89}Zr -REGN3504 in the NCI-H441, HCC827 and MDA-MB-231 studies, respectively. PD-L1, programmed death-ligand 1.

and PD-1 to determine the ability of ^{89}Zr -REGN3504 to detect expression of PD-L1 in normal tissues and to model the effect of normal tissue expression on tumor localization of the antibody. Prominent expression of PD-L1 in the humanized mice was evident by rapid target mediated

clearance of 0.1 mg/kg ^{89}Zr -REGN3504 from the circulation at early time points post injection and the rapid accumulation of ^{89}Zr signal in the spleen (figure 3A,B). Clear localization of ^{89}Zr -REGN3504 to the lymph nodes was also apparent from ex vivo biodistribution results. Increasing

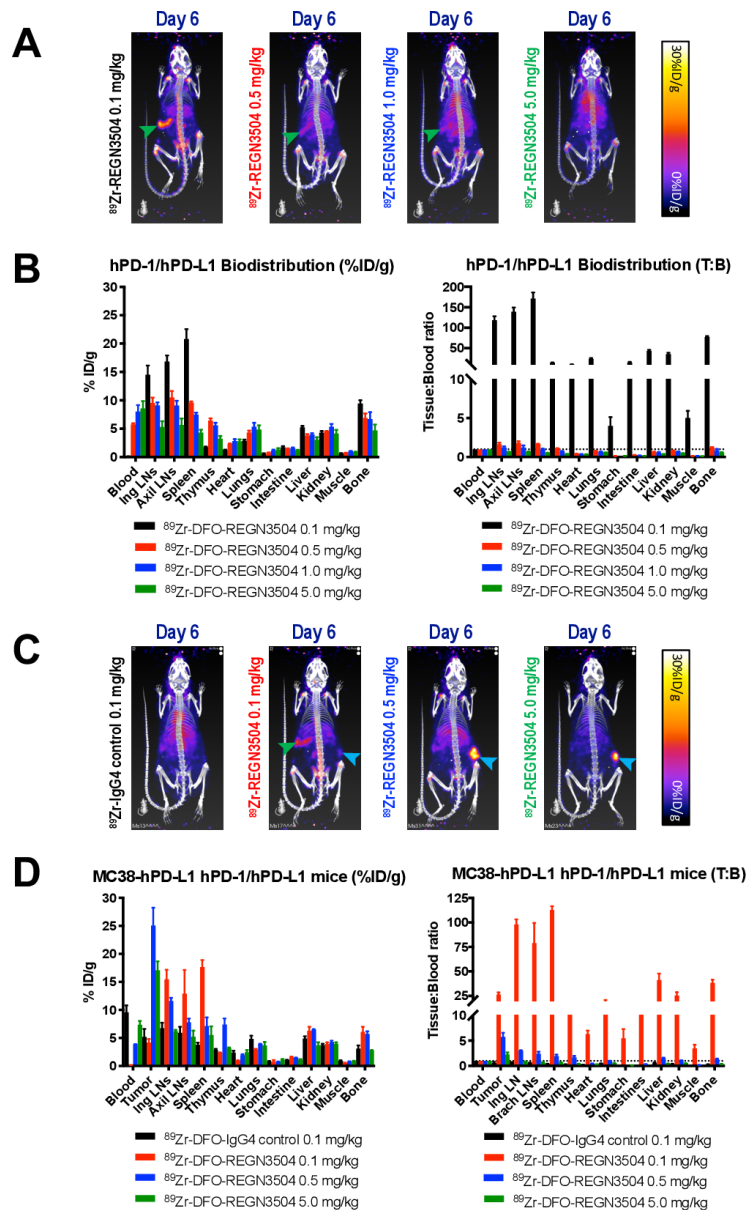


Figure 3 ^{89}Zr -REGN3504 demonstrates specific localization to PD-L1 positive tissues and targeting to MC38/hPD-L1 tumors in PD-1/hPD-L1 double humanized mice. The localization of ^{89}Zr -REGN3504 was assessed in mice humanized for PD-1 and PD-L1 (n=4/group). Animals received a single intravenous injection ^{89}Zr -REGN3504 (1.3 MBq) and PET/CT images were acquired on Day 0, 1, 4 and 6 Days post injection. On Day 6 post injection, quantitative ex vivo biodistribution was performed. Representative PET/CT images demonstrate the localization ^{89}Zr -REGN3504 on Day 6 for mice that received total antibody doses (^{89}Zr -REGN3504 0.1 mg/kg plus additional REGN3504) of 0.1, 0.5, 1.0 and 5 mg/kg (A). The biodistribution for these mice presented as per cent injected dose per gram (%ID/g) or tissue-to-blood ratio (T:B) is shown in B. The tumor localization and biodistribution of ^{89}Zr -REGN3504 was also assessed in mice humanized for PD-1 and PD-L1 bearing MC38/hPD-L1 tumors (n=4/group). Animals received a single intravenous injection ^{89}Zr -IgG4 control (1.37 MBq) or ^{89}Zr -REGN3504 (1.18 MBq) and PET/CT images were acquired on Day 0, 1, 4 and 6 Days post injection. On Day 6 post injection, quantitative ex vivo biodistribution was performed. Representative PET/CT images demonstrate the localization of ^{89}Zr -IgG4 control or ^{89}Zr -REGN3504 on Day 6 for mice that received 0.1 mg/kg ^{89}Zr -IgG4 control or ^{89}Zr -REGN3504 at total antibody doses (^{89}Zr -REGN3504 0.1 mg/kg plus additional REGN3504) of 0.1, 0.5, and 5 mg/kg (C). The biodistribution for these mice presented as per cent injected dose per gram (%ID/g) or tissue-to-blood ratio (T:B) is shown in D. Arrows highlight spleen (green arrow) and tumor (blue arrow) uptake. PD-1, programmed cell death protein 1; PD-L1, programmed death-ligand 1.

total REGN3504 antibody doses by the addition of unlabeled antibody led to rapid increases in ^{89}Zr -REGN3504 blood levels and an associated decrease in specific uptake in tissue due to competition. Biodistribution results also suggested specific uptake of ^{89}Zr -REGN3504 in the thymus and possibly liver, although absolute levels were moderate and below the respective level in blood. Uptake was also apparent in bone, possibly due to catabolism of ^{89}Zr -REGN3504 and retention of free ^{89}Zr .³⁹

To understand the localization of ^{89}Zr -REGN3504 in PD-L1 positive tumors relative to normal tissue, studies were next performed in humanized mice bearing MC-38/hPD-L1 tumors (figure 3C and D). At the lowest dose of 0.1 mg/kg ^{89}Zr -REGN3504, no significant localization to tumor was apparent, most likely due to rapid target mediated clearance and distribution of antibody to lymphoid tissues as observed in tumor-free mice. However, when the overall antibody dose was increased to 0.5 mg/kg, significant tumor localization by ^{89}Zr -REGN3504 was apparent and was accompanied by a clear reduction in uptake in lymphoid tissues. At an antibody dose of 5 mg/kg ^{89}Zr -REGN3504, some uptake was observed in tumors but less than observed with 0.5 mg/kg ^{89}Zr -REGN3504. The reduced tumor and lymphoid uptake accompanied by higher blood levels suggests that excess unlabeled REGN3504 blocked localization of ^{89}Zr -REGN3504 to PD-L1 expressing tissues at this dose.

^{89}Zr -REGN3504 successfully detects dynamic changes in PD-L1 expression in clodronate treated PD-1/PD-L1 humanized mice

The ability of ^{89}Zr -REGN3504 to detect dynamic changes in PD-L1 expression in vivo was assessed by using clodronate liposomes to specifically deplete phagocytic myeloid cells that include PD-L1 positive cell populations. PD-1/PD-L1 double humanized mice were treated with clodronate liposomes or control liposomes (8 $\mu\text{l/g}$) 2 days before ^{89}Zr -REGN3504 administration and at 1 and 4 days post administration, in order to maintain depletion of phagocytic cells over the course of the 6-day imaging and biodistribution study. The ability of clodronate treatment to systemically deplete PD-L1 positive phagocytic cell populations in vivo was independently validated by flow cytometry of blood and spleens (online supplemental figure 6).

Consistent with earlier studies in non-liposome treated mice, rapid localization of ^{89}Zr -REGN3504 in the spleen was apparent in Day 1 imaging (figure 4A). Targeting of ^{89}Zr -REGN3504 to spleens was initially apparent in mice treated with both control and clodronate liposomes. However, at the later Day 4 and 6 time points, a clear reduction in spleen signal was apparent in clodronate treated mice. Images of ^{89}Zr -IgG4 control treated mice demonstrate gradual clearance of the antibody from heart and major vessels, without significant targeting of the spleen in both control and clodronate treated animals. Ex vivo biodistribution results confirmed that ^{89}Zr -REGN3504 uptake was reduced in spleens of clodronate treated mice,

with $8.9\% \pm 4.5\% \text{ID/g}$ observed in the spleens of these animals relative to $29.3\% \pm 1.8\% \text{ID/g}$ in control treated mice ($p=0.0012$) (figure 4B). A modest reduction in uptake was also apparent in lymph nodes of clodronate treated mice, with inguinal and brachial lymph node uptake reduced to $19.0\% \pm 6.1\% \text{ID/g}$ and $18.7\% \pm 3.9\% \text{ID/g}$ from $24.5\% \pm 8.0\% \text{ID/g}$ and $28.8\% \pm 7.4\% \text{ID/g}$, although this was not significant.

Dosimetry of ^{89}Zr -REGN3504 in PD-1/PD-L1 humanized mice

The time dependent biodistribution of ^{89}Zr -REGN3504 in mice was used to predict the whole body and tissue radiation dosimetry in human subjects. The estimated human tissue absorbed doses for ^{89}Zr -REGN3504 derived from PD-1/PD-L1 humanized mice that received 1 mg/kg (1.85 MBq) ^{89}Zr -REGN3504 are shown in table 1. The decay corrected VOI values from the study and the resulting human tissue mean residency times used for calculation of the estimated human dosimetry are shown in online supplemental tables 2 and 3. The overall effective human dose for ^{89}Zr -REGN3504 was estimated to be 0.513 mSv/MBq (millisievert/megabecquerel) in an adult male and 0.622 mSv/MBq in female. The organs predicted to have the highest absorbed dose in humans are the spleen and liver. For men, the absorbed dose in spleen and liver were 0.856 mSv/MBq and 0.764 mSv/MBq. The respective spleen and liver values for women were 1.12 mSv/MBq and 0.974 mSv/MBq.

Pharmacokinetics of REGN3504 in cynomolgus monkeys

As REGN3504 cross-reacts with cynomolgus monkey PD-L1 with similar binding affinity to human PD-L1, the pharmacokinetics of REGN3504 was assessed in female monkeys following a single intravenous administration at 1, 5 or 15 mg/kg. Concentration-time profiles following dosing were characterized by a brief distribution phase, followed by a linear beta elimination phase (figure 5). The onset of anti-drug antibody (ADA) formation and the resultant precipitous drop in REGN3504 serum concentrations obscured the terminal elimination kinetics. Subsequently, pharmacokinetic parameters were evaluated prior to the first apparent incidence of ADA following Day 8 of dosing. The dose-normalized exposures (AUC (area under the curve)/dose) across the dose groups were generally comparable and indicative of linear kinetics (online supplemental table 4).

DISCUSSION

We describe here a novel anti-PD-L1 immuno-PET agent, ^{89}Zr -REGN3504, that can sensitively detect human PD-L1 expression in vivo. Initial in vitro characterization of DFO-REGN3504 and radiolabeled ^{89}Zr -REGN3504 demonstrated that both retained the specific binding properties of the unmodified antibody. Antibody REGN3504 potentially blocked the interaction of PD-L1 with both PD-1 and CD80. Despite this activity, REGN3504 is not anticipated to have significant functional effects on tumors

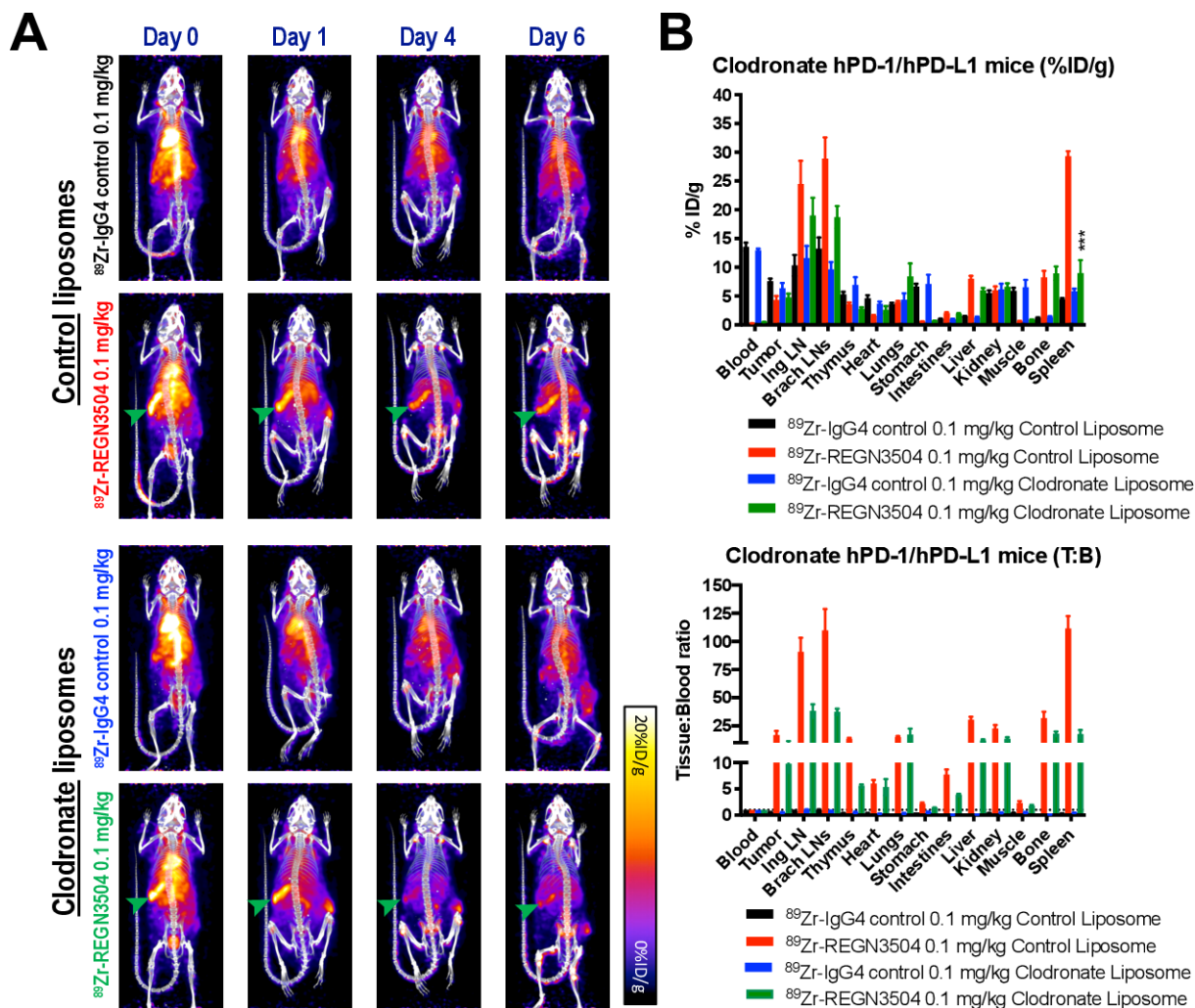


Figure 4 Localization of ^{89}Zr -REGN3504 is reduced in the spleens of PD-1/PD-L1 humanized mice treated with clodronate liposomes. The tumor localization and biodistribution of ^{89}Zr -REGN3504 was also assessed in mice humanized for PD-1 and PD-L1 bearing MC-38/hPD-L1 tumors following treatment with control or clodronate liposomes ($n=4$). Animals were treated with clodronate liposomes or control liposomes ($8\mu\text{l/g}$) 2 days before ^{89}Zr -antibody administration and 1 and 4 days post injection. Animals received a single intravenous injection of 0.1 mg/kg ^{89}Zr -IgG4 control (1.3 MBq) or 0.1 mg/kg ^{89}Zr -REGN3504 (1.3 MBq) and PET/CT images were acquired on Day 0, 1, 4 and 6 Days post-injection. On Day 6 post injection, quantitative ex vivo biodistribution was performed. Representative PET/CT images demonstrate the localization of 0.1 mg/kg ^{89}Zr -IgG4 control or ^{89}Zr -REGN3504 over time in control or clodronate treated animals (A). The biodistribution for these mice presented as per cent injected dose per gram (%ID/g) or tissue-to-blood ratio (T:B) is shown in B. Arrows highlight spleen (green arrow) uptake. PD-1, programmed cell death protein 1; PD-L1, programmed death-ligand 1.

in the context of immuno-PET, as imaging uses a mass dose of antibody that is generally below that required for therapeutic activity of PD-L1 antibodies.^{40–41} Further, REGN3504 is a human IgG4 and therefore has reduced effector functions relative to an IgG1 isotype.

Using immuno-PET or related imaging techniques such as immuno-SPECT, PD-L1 expression has been assessed in preclinical studies using antibodies directed against both mouse and human PD-L1.^{42–43} These studies have demonstrated the general feasibility of detecting PD-L1 expression in both select normal tissues and in tumor models via antibody imaging. As REGN3504 does not bind murine PD-L1, we initially assessed the ability of ^{89}Zr -REGN3504 to detect PD-L1 in vivo using mice bearing human tumor xenografts, where sensitive and

specific detection of PD-L1 expression in the xenografts was apparent. Interestingly, specific detection of PD-L1 was observed despite relatively low expression of PD-L1 in the xenografts as detected by immunohistochemistry with the clinically used SP263 antibody. It's possible that internalization of ^{89}Zr -REGN3504 and the subsequent intracellular retention of ^{89}Zr may serve to amplify the PET signal and increase sensitivity of the PD-L1 detection.⁴¹

The xenograft studies however have the limitation of not being able to discern the effect of PD-L1 expression in normal tissues on tumor uptake due to the lack of REGN3504 binding to murine PD-L1. We therefore generated mice expressing human PD-1 and PD-L1 to allow the study of ^{89}Zr -REGN3504 targeting to normal sites of PD-L1 expression. In tumor-free humanized mice,

Table 1 Estimated human tissue absorbed doses and effective dose for ⁸⁹Zr-DFO-REGN3054

Organ/tissue	Physical decay*		Biexponential fit†	
	Adult male (mSv/MBq)	Adult female (mSv/MBq)	Adult male (mSv/MBq)	Adult female (mSv/MBq)
Adrenals	0.561	0.702	0.567	0.726
Brain	0.179	0.237	0.182	0.234
Breasts	0.366	0.459	0.379	0.466
Gallbladder wall	0.601	0.692	0.610	0.751
LLI wall	0.519	0.652	0.530	0.651
Small intestine	0.563	0.600	0.582	0.605
Stomach wall	0.575	0.714	0.584	0.718
ULI wall	0.553	0.685	0.571	0.700
Heart wall	0.789	0.973	0.781	0.964
Kidney	0.650	0.773	0.641	0.774
Liver	0.764	0.974	0.764	1.220
Lungs	0.575	0.705	0.561	0.700
Muscle	0.396	0.481	0.381	0.464
Ovaries	0.533	0.645	0.542	0.642
Pancreas	0.597	0.743	0.606	0.765
Red marrow	0.480	0.591	0.483	0.587
Osteogenic cells	0.604	0.777	0.625	0.779
Skin	0.291	0.373	0.297	0.374
Spleen	0.856	1.120	0.876	1.160
Testes	0.399	NA	0.407	NA
Thymus	0.481	0.605	0.484	0.601
Thyroid	0.417	0.484	0.423	0.480
Urinary bladder wall	0.580	0.496	0.559	0.494
Uterus	0.545	0.638	0.554	0.636
Total body	0.440	0.550	0.440	0.554
Effective dose	0.513	0.622	0.516	0.625

*Absorbed doses calculated from MRT assuming only physical decay following day 6 time point.

†Absorbed doses calculated from MRT with a biexponential fit of the data.

LLI, lower large intestine; MRT, mean residence time; mSv/MBq, millisievert/megabecquerel; NA, not applicable; ULI, upper large intestine.

rapid targeting of ⁸⁹Zr-REGN3504 to the spleen and lymph nodes was observed. These results were consistent with other preclinical reports assessing radiolabeled anti-PD-L1 antibodies that have demonstrated that spleen and lymph nodes are the predominant sites of PD-L1 expression in mice.^{42–44–46} Accordingly, localization of ⁸⁹Zr-REGN3504 to spleen was most significantly affected by systemic depletion of PD-L1-expressing phagocytic cells following treatment with clodronate liposomes. Further, the reduced splenic uptake of ⁸⁹Zr-REGN3504 following clodronate treatment validates that it can sensitively detect dynamic changes in PD-L1 positive cell populations in vivo.

Interestingly, some studies have reported localization of anti-PD-L1 antibodies to brown adipose tissue in addition to lymphoid organs.⁴⁷ However, our imaging did not demonstrate any specific localization of ⁸⁹Zr-REGN3504

to brown adipose tissues. Further, tissue-to-blood ratios did not demonstrate evidence of specific uptake in tissues such as the lungs, small intestine or liver. Specific localization of antibody to brown adipose tissue was not reported in a study assessing murine PD-L1 reactive ⁸⁹Zr-Avelumab, which otherwise demonstrated localization to the spleen and lymph nodes of mice.⁴⁴ The use of different antibodies, antibody doses and mouse strains across these studies makes detailed comparison of the results difficult. Further studies in humanized mice bearing MC-38 tumors expressing human PD-L1 demonstrate the importance of normal tissues expression on the degree of tumor targeting by ⁸⁹Zr-REGN3504. With a low dose of ⁸⁹Zr-REGN3504 (0.1 mg/kg), minimal accumulation in MC-38/hPD-L1 tumors was observed, suggesting that rapid localization to lymphoid tissues impeded slower localization to tumors. Increasing the overall protein dose of ⁸⁹Zr-REGN3504 to 0.5 or 5 mg/kg led to improved blood levels

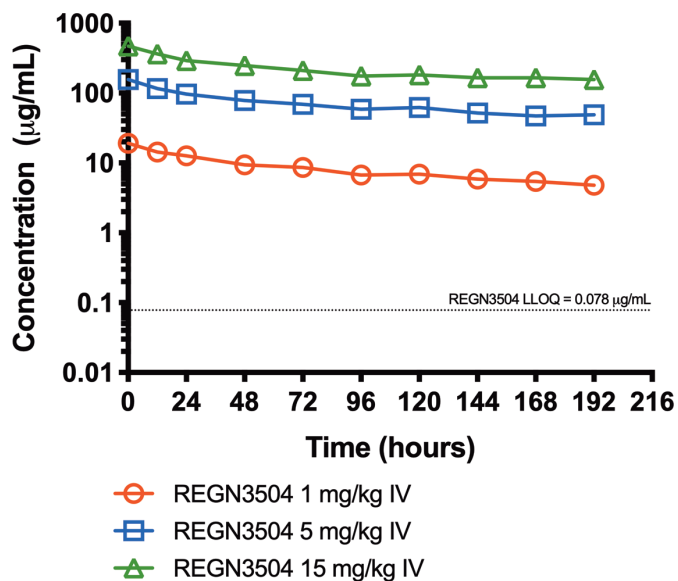


Figure 5 Concentration-time profiles of REGN3504 in cynomolgus monkeys. Concentrations of REGN3504 in serum versus time through 8 Days following a single intravenous infusion of REGN3504 at 1, 5 or 15 mg/kg in female cynomolgus monkeys. Values are mean \pm SD IV, intravenous.

and increased tumor uptake. Overall, these studies highlight that sufficient antibody concentrations are required to overcome distribution to PD-L1 positive normal tissues in order to provide circulating ^{89}Zr -REGN3504 levels required for specific tumor accumulation.^{42 45 46}

Dose optimization is a standard component of initial immuno-PET clinical studies.^{28 30} The predicted human absorbed effective doses for ^{89}Zr -REGN3504 were moderate and generally consistent with those known to be safe from previous applications of immuno-PET utilizing ^{89}Zr in humans. Despite the clear expression of PD-L1 in normal tissues, the apparent linear kinetics and lack of obvious target-mediated clearance of REGN3504 as observed over the 1 to 15 mg/kg range in cynomolgus monkeys (for the duration of observed concentrations) suggest that overall levels are moderate. Overall, our characterization of REGN3504 together with the wider clinical experience with anti-PD-L1 therapeutics further supports the continued development of ^{89}Zr -REGN3504.

A recent study demonstrated the potential of immuno-PET for monitoring and predicting the response to anti-PD-L1 immunotherapy. ^{89}Zr -atezolizumab was tested in 22 patients with either bladder cancer, triple-negative breast cancer or NSCLC prior to atezolizumab therapy.⁴¹ Promisingly, imaging with ^{89}Zr -atezolizumab immuno-PET resulted in high but variable uptake in tumors that better correlated with clinical responses than IHC or RNA-sequencing based approaches. Another recent study showed that partial responses to nivolumab were associated with increased tumor uptake of either ^{89}Zr -nivolumab or the adnectin based anti-PD-L1 PET agent ^{18}F -BMS-986192.⁴⁸ Although immuno-PET with whole IgG imaging agents requires time to distribute and clear for optimal imaging 4 to 7 days after administration, it may

provide a good correlate to the distribution and accessibility of antibody-based immunotherapies.^{16 42} Anti-PD-1 antibody cemiplimab was approved in late 2018 for the treatment of metastatic cutaneous squamous cell carcinoma and is in further clinical development in an array of other tumor types as a monotherapy and in combination with both established and experimental cancer therapeutics.^{38 49} A first-in-human qualification clinical study (NCT03746704) has been initiated to evaluate the safety, optimal mass dose and uptake time, biodistribution and targeting of ^{89}Zr -REGN3504. Future clinical studies with ^{89}Zr -REGN3504 could allow the assessment of whole-body PD-L1 expression in patients receiving cemiplimab immunotherapy alone or in combination with other therapeutic drugs.

Acknowledgements We thank all the Regeneron employees who contributed to the generation and characterization of ^{89}Zr -DFO-REGN3504 including Lauren Havel, Erica Ullman, Aynur Hermann, Celestine Thomas, Tammy Huang, Ashique Rafique, Joel Martin, Peter Hong, Elena Burova and Ella Ioffe. We would also like to thank Kelly Orcutt and Andrew Novicki from Invivo for their assistance with the human dosimetry estimation studies. We thank Dinko Gonzalez Trotter for reviewing and editing the manuscript.

Contributors MPK wrote the manuscript, led the study design and conceptualization, performed animal studies, imaging, ex vivo studies and data analysis. SM, CH and MD performed animal studies, imaging, and ex vivo studies. TCA and JTG performed antibody conjugation, radiolabelings and radio-conjugate characterization. CG, IC and DD performed the in vitro assessment of REGN3504 and DFO-REGN3504. MWR performed the PK analysis of REGN3504. RT participated in study design and conceptualization, in vivo studies and review of the manuscript. DM, WCO, GT and JRK participated in study design and conceptualization, supervision of the studies and review of the manuscript.

Funding This work was funded exclusively by Regeneron Pharmaceuticals.

Competing interests We have no conflicts of interests to disclose, other than our employment at Regeneron Pharmaceuticals.

Patient consent for publication Not required.

Provenance and peer review Not commissioned; externally peer reviewed.

Data availability statement Data are available upon reasonable request.

Supplemental material This content has been supplied by the author(s). It has not been vetted by BMJ Publishing Group Limited (BMJ) and may not have been peer-reviewed. Any opinions or recommendations discussed are solely those of the author(s) and are not endorsed by BMJ. BMJ disclaims all liability and responsibility arising from any reliance placed on the content. Where the content includes any translated material, BMJ does not warrant the accuracy and reliability of the translations (including but not limited to local regulations, clinical guidelines, terminology, drug names and drug dosages), and is not responsible for any error and/or omissions arising from translation and adaptation or otherwise.

Open access This is an open access article distributed in accordance with the Creative Commons Attribution Non Commercial (CC BY-NC 4.0) license, which permits others to distribute, remix, adapt, build upon this work non-commercially, and license their derivative works on different terms, provided the original work is properly cited, appropriate credit is given, any changes made indicated, and the use is non-commercial. See <http://creativecommons.org/licenses/by-nc/4.0/>.

ORCID iDs

Marcus P Kelly <http://orcid.org/0000-0002-1276-3107>

Drew Dudgeon <http://orcid.org/0000-0002-2934-0127>

REFERENCES

- Fritz JM, Lenardo MJ. Development of immune checkpoint therapy for cancer. *J Exp Med* 2019;216:1244–54.
- Sharma P, Allison JP. The future of immune checkpoint therapy. *Science* 2015;348:56–61.
- Pardoll DM. The blockade of immune checkpoints in cancer immunotherapy. *Nat Rev Cancer* 2012;12:252–64.

- 4 Wei SC, Duffy CR, Allison JP. Fundamental mechanisms of immune checkpoint blockade therapy. *Cancer Discov* 2018;8:1069–86.
- 5 Ancevski Hunter K, Socinski MA, Villaruz LC. Pd-L1 testing in guiding patient selection for PD-1/PD-L1 inhibitor therapy in lung cancer. *Mol Diagn Ther* 2018;22:1–10.
- 6 Havel JJ, Chowell D, Chan TA. The evolving landscape of biomarkers for checkpoint inhibitor immunotherapy. *Nat Rev Cancer* 2019;19:133–50.
- 7 Patel SP, Kurzrock R. Pd-L1 expression as a predictive biomarker in cancer immunotherapy. *Mol Cancer Ther* 2015;14:847–56.
- 8 Topalian SL, Hodi FS, Brahmer JR, et al. Safety, activity, and immune correlates of anti-PD-1 antibody in cancer. *N Engl J Med* 2012;366:2443–54.
- 9 Taube JM, Klein A, Brahmer JR, et al. Association of PD-1, PD-1 ligands, and other features of the tumor immune microenvironment with response to anti-PD-1 therapy. *Clin Cancer Res* 2014;20:5064–74.
- 10 Herbst RS, Baas P, Kim D-W, et al. Pembrolizumab versus docetaxel for previously treated, PD-L1-positive, advanced non-small-cell lung cancer (KEYNOTE-010): a randomised controlled trial. *Lancet* 2016;387:1540–50.
- 11 Reck M, Rodríguez-Abreu D, Robinson AG, et al. Pembrolizumab versus chemotherapy for PD-L1-positive non-small-cell lung cancer. *N Engl J Med* 2016;375:1823–33.
- 12 Daud AI, Wolchok JD, Robert C, et al. Programmed death-ligand 1 expression and response to the Anti-Programmed death 1 antibody pembrolizumab in melanoma. *J Clin Oncol* 2016;34:4102–9.
- 13 Rittmeyer A, Barlesi F, Waterkamp D, et al. Atezolizumab versus docetaxel in patients with previously treated non-small-cell lung cancer (oak): a phase 3, open-label, multicentre randomised controlled trial. *Lancet* 2017;389:255–65.
- 14 Shukuya T, Carbone DP. Predictive markers for the efficacy of anti-PD-1/PD-L1 antibodies in lung cancer. *J Thorac Oncol* 2016;11:976–88.
- 15 Balar AV, Galsky MD, Rosenberg JE, et al. Atezolizumab as first-line treatment in cisplatin-ineligible patients with locally advanced and metastatic urothelial carcinoma: a single-arm, multicentre, phase 2 trial. *Lancet* 2017;389:67–76.
- 16 Verhoeff SR, van den Heuvel MM, van Herpen CML, et al. Programmed cell death-1/ligand-1 PET imaging: a novel tool to optimize immunotherapy? *PET Clin* 2020;15:35–43.
- 17 Callea M, Albiges L, Gupta M, et al. Differential expression of PD-L1 between primary and metastatic sites in clear-cell renal cell carcinoma. *Cancer Immunol Res* 2015;3:1158–64.
- 18 Hofman P. The challenges of evaluating predictive biomarkers using small biopsy tissue samples and liquid biopsies from non-small cell lung cancer patients. *J Thorac Dis* 2019;11:S57–64.
- 19 Ilie M, Long-Mira E, Bence C, et al. Comparative study of the PD-L1 status between surgically resected specimens and matched biopsies of NSCLC patients reveal major discordances: a potential issue for anti-PD-L1 therapeutic strategies. *Ann Oncol* 2016;27:147–53.
- 20 Kluger HM, Zito CR, Turcu G, et al. Pd-L1 studies across tumor types, its differential expression and predictive value in patients treated with immune checkpoint inhibitors. *Clin Cancer Res* 2017;23:4270–9.
- 21 Hirsch FR, McElhinny A, Stanforth D, et al. Pd-L1 immunohistochemistry assays for lung cancer: results from phase 1 of the blueprint PD-L1 IHC assay comparison project. *J Thorac Oncol* 2017;12:208–22.
- 22 Hato SV, Khong A, de Vries IJM, et al. Molecular pathways: the immunogenic effects of platinum-based chemotherapeutics. *Clin Cancer Res* 2014;20:2831–7.
- 23 Kondo A, Yamashita T, Tamura H, et al. Interferon-Gamma and tumor necrosis factor-alpha induce an immunoinhibitory molecule, B7-H1, via nuclear factor-kappaB activation in blasts in myelodysplastic syndromes. *Blood* 2010;116:1124–31.
- 24 Twyman-Saint Victor C, Rech AJ, Maity A, et al. Radiation and dual checkpoint blockade activate non-redundant immune mechanisms in cancer. *Nature* 2015;520:373–7.
- 25 Alauddin MM, Khawli LA. Advances in Immuno-PET in the detection of cancer and assessment of response to therapy. *Curr Med Chem* 2020. doi:10.2174/0929867327666200128102958. [Epub ahead of print: 27 Jan 2020].
- 26 Broos K, Lecocq Q, Raes G, et al. Noninvasive imaging of the PD-1:PD-L1 immune checkpoint: embracing nuclear medicine for the benefit of personalized immunotherapy. *Theranostics* 2018;8:3559–70.
- 27 Marciscano AE, Thorek DLJ. Role of noninvasive molecular imaging in determining response. *Adv Radiat Oncol* 2018;3:534–47.
- 28 Jauw YWS, Menke-van der Houven van Oordt CW, Hoekstra OS, et al. Immuno-positron emission tomography with Zirconium-89-Labeled monoclonal antibodies in oncology: what can we learn from initial clinical trials? *Front Pharmacol* 2016;7:131.
- 29 Lamberts LE, Williams SP, Terwisscha van Scheltinga AGT, et al. Antibody positron emission tomography imaging in anticancer drug development. *J Clin Oncol* 2015;33:1491–504.
- 30 Van Dongen GA, Huisman MC, Boellaard R, et al. 89Zr-immuno-PET for imaging of long circulating drugs and disease targets: why, how and when to be applied? *Q J Nucl Med Mol Imaging* 2015;59:18–38.
- 31 van Dongen GAMS, Visser GWM, Lub-de Hooge MN, et al. Immuno-PET: a navigator in monoclonal antibody development and applications. *Oncologist* 2007;12:1379–89.
- 32 Moek KL, Giesen D, Kok IC, et al. Theranostics using antibodies and antibody-related therapeutics. *J Nucl Med* 2017;58:83S–90.
- 33 Waaijer SJH, Kok IC, Eisses B, et al. Molecular imaging in cancer drug development. *J Nucl Med* 2018;59:726–32.
- 34 Wu AM. Antibodies and antimatter: the resurgence of immuno-PET. *J Nucl Med* 2009;50:2–5.
- 35 Murphy AJ, Macdonald LE, Stevens S, et al. Mice with megabase humanization of their immunoglobulin genes generate antibodies as efficiently as normal mice. *Proc Natl Acad Sci U S A* 2014;111:5153–8.
- 36 Poueymirou WT, Auerbach W, Frendewey D, et al. F0 generation mice fully derived from gene-targeted embryonic stem cells allowing immediate phenotypic analyses. *Nat Biotechnol* 2007;25:91–9.
- 37 Valenzuela DM, Murphy AJ, Frendewey D, et al. High-Throughput engineering of the mouse genome coupled with high-resolution expression analysis. *Nat Biotechnol* 2003;21:652–9.
- 38 Burova E, Hermann A, Waite J, et al. Characterization of the anti-PD-1 antibody REGN2810 and its antitumor activity in human PD-1 knock-in mice. *Mol Cancer Ther* 2017;16:861–70.
- 39 Wei W, Rosenkrans ZT, Liu J, et al. ImmunoPET: concept, design, and applications. *Chem Rev* 2020;120:3787–851.
- 40 Warram JM, de Boer E, Sorace AG, et al. Antibody-based imaging strategies for cancer. *Cancer Metastasis Rev* 2014;33:809–22.
- 41 Bensch F, van der Veen EL, Lub-de Hooge MN, et al. ⁸⁹Zr-atezolizumab imaging as a non-invasive approach to assess clinical response to PD-L1 blockade in cancer. *Nat Med* 2018;24:1852–8.
- 42 Heskamp S, Wierstra PJ, Molkenboer-Kuennen JDM, et al. Pd-L1 microSPECT/CT imaging for longitudinal monitoring of PD-L1 expression in syngeneic and humanized mouse models for cancer. *Cancer Immunol Res* 2019;7:150–61.
- 43 Hettich M, Braun F, Bartholomä MD, et al. High-resolution PET imaging with therapeutic antibody-based PD-1/PD-L1 checkpoint tracers. *Theranostics* 2016;6:1629–40.
- 44 Jagoda EM, Vasalatiy O, Basuli F, et al. Immuno-PET imaging of the programmed cell death-1 ligand (PD-L1) using a Zirconium-89 labeled therapeutic antibody, Avelumab. *Mol Imaging* 2019;18:1536012119829986.
- 45 Josefsson A, Nedrow JR, Park S, et al. Imaging, biodistribution, and dosimetry of radionuclide-Labeled PD-L1 antibody in an immunocompetent mouse model of breast cancer. *Cancer Res* 2016;76:472–9.
- 46 Nedrow JR, Josefsson A, Park S, et al. Imaging of programmed cell death ligand 1: impact of protein concentration on distribution of anti-PD-L1 SPECT agents in an immunocompetent murine model of melanoma. *J Nucl Med* 2017;58:1560–6.
- 47 Ingram JR, Dougan M, Rashidian M, et al. PD-L1 is an activation-independent marker of brown adipocytes. *Nat Commun* 2017;8:647.
- 48 Niemeijer AN, Leung D, Huisman MC, et al. Whole body PD-1 and PD-L1 positron emission tomography in patients with non-small-cell lung cancer. *Nat Commun* 2018;9:4664.
- 49 Migden MR, Rischin D, Schmults CD, et al. PD-1 blockade with cemiplimab in advanced cutaneous squamous-cell carcinoma. *N Engl J Med* 2018;379:341–51.